Journal of Chromatography A 1769 (2026) 466706

Contents lists available at ScienceDirect

Journal of Chromatography A

journal homepage: www.elsevier.com/locate/chroma

Molecular dynamics simulations elucidate the structural determinants of size-exclusion chromatography behavior in dimeric G-quadruplex-RHAU

Min Zhu [a], Long-yu Zhu [a], Lu-yan An [a], Ju Wang [a], Jun-qin Qiao [a,*], Han-yue Yang [b,*], Wei-juan Zheng [c], Hong-zhen Lian [a,*]

[a] State Key Laboratory of Analytical Chemistry for Life Science, School of Chemistry & Chemical Engineering and Centre for Shared Scientific Research Facilities, Nanjing University, 163 Xianlin Avenue, Nanjing 210023, China
[b] Jiangsu Deyuan Pharmaceutical Co., Ltd., 21 Jinqiao Road, Lianyungang 222002, China
[c] State Key Laboratory of Pharmaceutical Biotechnology, School of Life Sciences, Nanjing University, 163 Xianlin Avenue, Nanjing 210023, China

ARTICLE INFO

Keywords:
Dimeric G-quadruplexes
RHAU
Molecular dynamics simulations
Retention behavior
Interaction mechanisms

ABSTRACT

Research on G-quadruplexes (G4s)-RNA helicase associated with AU-rich element (RHAU) interaction has facilitated G4s-targeted therapeutic development. Despite this progress, the interaction between dimeric G-quadruplexes (D-G4s) and RHAU remain less explored compared to monomeric structures. Developing convenient and visual methods to elucidate the interaction mechanisms between different D-G4s structures and RHAU can provide new insights into binding modes, thus aiding in the design of molecular tools targeting D-G4s. In this study, we combined molecular dynamics (MD) simulations with size-exclusion chromatography (SEC) and isothermal titration calorimetry (ITC) to investigate structural dependencies in D-G4s-RHAU interactions for the first time. Diverse D-G4s included hybrid non-parallel (D-24TTG), intramolecular tandem parallel (dAGRO100, GGA8), interlocking parallel (93del), and intermolecular stacked parallel (T30695, T30177) structures were analyzed. MD simulations revealed that the distinct SEC retention behaviors in D-G4s-RHAU interactions were mainly governed by binding site accessibility, inter-site steric hindrance, and binding free energy gradients, trends supported by ITC measured affinities. Furthermore, energy decomposition analysis identified Glu26 in RHAU as a critical residue contributing to electrostatic interactions. Mutating to Arg26 substantially decreased the binding free energy (-94.05 ± 0.41 kJ/mol), emphasizing its functional importance. Thus, this work demonstrates that MD simulations are indispensable for revealing the causes of experimental phenomena and understanding the mechanisms underlying chromatographic behavior. This combined strategy not only discerns interaction patterns stemming from structural diversity but facilitates the rapid screening of G4s-targeting molecules.

1. Introduction

G-quadruplexes (G4s), non-canonical nucleic acid secondary structures formed by guanine-rich sequences [1], are abundant in genomic regulatory regions including telomeres, oncogene promoters, and mRNA untranslated regions, where they play an important role in modulated critical biological functions [2–4]. As prevalent multimer, dimeric G4s (D-G4s) represent promising targets for developing selective therapeutics [5,6] and functional nanomaterials. The structural elucidation of D-G4s could enable ligand design for gene expression regulation [7] and enhance their application in DNA nanotechnology for targeted delivery systems [8].

The RNA helicase associated with AU-rich element (RHAU) peptide has been demonstrated to exhibit G4s helicase enzyme activity, which enables to bind and unwind G4s structures in DNA and RNA [9,10]. Exploring the interaction between RHAU and D-G4s can reveal how the peptide selectively recognizes and binds to these nucleic acid structures. Designing functional proteins which specifically targeting D-G4s for the regulation of G4s-associated biological processes, such as inhibition of protein expression [11], provides new strategies for disease treatment. Additionally, such research may provide a structural basis and theoretical guidance for developing novel G4s ligands to be used in chemical biology research, like the monitoring and regulation of G4s-related biological processes [12,13], as well as the development of

* Corresponding authors.
E-mail addresses: qiaojunqin@nju.edu.cn (J.-q. Qiao), yanghanyue@pharmdy.com (H.-y. Yang), hzlian@nju.edu.cn (H.-z. Lian).

https://doi.org/10.1016/j.chroma.2026.466706
Received 11 November 2025; Received in revised form 9 January 2026; Accepted 11 January 2026
Available online 12 January 2026

G4s-targeted drugs [14]. This is exemplified by the strategy of targeting G4s structures in oncogene promoters (e.g., MYC, KRAS) to address challenging drug-resistant proteins, where natural product derived ligands show significant potential [15].

Current methodologies for studying G4s-RHAU interactions mainly include circular dichroism spectroscopy for structural characterization [16,17], X-ray crystallography for the visualization of complexes at atomic resolution [18,19], and fluorescent probes for monitoring G4s in cells [20], etc. Our group have introduced size-exclusion chromatography (SEC) as a rapid analytical tool to study the interaction between RHAU and G4s with varying conformations [21]. While these methods offer valuable structural insights or capture ensemble-averaged dynamic properties, they generally lack the temporal resolution on binding dynamics. Molecular dynamics (MD) simulations complement these methods by offering a unique insight into the binding mechanism through time-resolved modelling of biomolecular dynamics [22,23].

In this work, the interaction between RHAU and D-G4s was simulated with MD to elucidate the detailed mechanism behind the D-G4s retention behavior exhibited in SEC. Our goal is to clarify the important modes and energy contributions during the binding process. By combining experimental results with computational simulations, a more comprehensive understanding of the G4s-RHAU binding mechanism can be achieved, potentially offering a novel strategy for exploring the particular structure of G4s. Furthermore, this approach could also provide more diversified options for G4s targeted drug development and biotechnology applications.

2. Materials and methods

2.1. Simulated systems

Six D-G4s-RHAU systems were focused on: D-24TTG [24], dAGRO100 [25], GGA8 [26], 93del [27], T30695 [28], and T30177 [29], along with one monomer G4s-RHAU system: 24TTG [30]. In addition to D-24TTG, which was constructed using Pymol 2.5 software [31] and assisted by 3D-NuS (https://www.iith.ac.in/3dnus) [32], other structures were derived from the RCSB database (https://www.rcsb.org/pdb) [33]. Comprehensive details concerning these structures were provided in Table 1, with a corresponding schematic diagram shown in Figure S1.

2.2. Molecular docking and MD simulations

The binding mode was explored with the HDOCK server (http://hdock.phys.hust.edu.cn) [34]. The top ten docking results were selected for comparative analysis to acquire representative structures for subsequent dynamics simulations.

Complexes with typical conformations obtained by docking were used as initial structures for the MD simulation. These models were placed in a cubic water box with the TIP3P model [35], under periodic boundary conditions. To more accurately reflect the conditions of SEC research, a salt solution with an ionic concentration of 0.10 M (comprising K^+ and Cl^-) incorporated into the simulated system. The MD simulations were achieved under the amber14sb_OL15 force field [36] by using the GROMACS 2019 software package [37,38]. Remote electrostatic interactions and van der Waals interactions were treated by the Particle-Mesh Ewald (PME) [39] method with a cut-off distance of 10 Å. After energy minimisation, a 500 ps pre-equilibration was conducted, and then the 500 ns MD simulation was performed at 303.15 K within the NPT ensemble [40] using a time step of 2.0 fs. Visualization of the trajectories and extraction of snapshots were carried by using the VMD 1.9.3 software [41].

Subsequently, the molecular mechanics/generalised Born surface area (MM/GBSA) method [42] was applied to analyse the binding free energy between RHAU and various D-G4s systems. The final 200 ns from each MD trajectory was selected, and 200 snapshots at 1 ns interval were extracted for subsequent calculations via gmx_MMPBSA [43]. The interacting bases or residues within a 3 Å binding range were subjected to energy decomposition.

2.3. Size exclusion chromatographic conditions

SEC was performed on an Agilent 1200 series HPLC, and chromatographic separation of the samples was achieved on a TSK_{gel} $G2000SW_{XL}$ column (300 × 7.8 mm i.d.), with column temperature maintained at 30 °C. Isocratic elution was performed at a flow rate of 0.5 mL min^{-1}, with 50 mM KH_2PO_4 (pH 7.0, adjusted by KOH) as mobile phase. The injection volume was 10 μL, and the detection wavelength was set at 260 nm. G4s concentration was fixed at 10 μM for all samples, and the molar ratios of D-G4s:RHAU in the complex system were set as 1:0, 1:1, 1:2, and 1:4, respectively. The specific chromatographic conditions and related data were referenced from the work of Wang et al. from our group [44].

2.4. Isothermal titration calorimetry conditions

A stock solution of RHAU (10 mM) was prepared by dissolution in ultrapure water and stored at −80 °C. The synthesized oligonucleotides were dissolved in a 10 mM potassium phosphate buffer (K_2HPO_4/KH_2PO_4, pH 7.0) containing 100 mM KCl to obtain a 300 μM DNA stock solution. Both stock solutions were diluted to the required working concentrations as needed. The diluted DNA solutions were annealed by heating at 95 °C for 10 min, followed by gradual cooling to room temperature. The annealed samples were then stored at 4 °C overnight. Isothermal titration calorimetry (ITC) measurements were carried out on a MicroCal iTC200 system at 25 °C. The RHAU solution (300 μM) was titrated into the G4s solution (20 μM) via 20 successive injections of 2 μL each, with a spacing of 300 s between injections. The stirring speed was maintained at 1000 rpm. The resulting titration data were fitted using the iTC200 with the Origin plug-in.

3. Results and discussion

3.1. Molecular docking

The HDOCK results were presented in Figure S2. Representative structures were chosen for further analysis. The interaction between D-24TTG and RHAU exhibited two distinct binding modes: vertical lateral binding and horizontal binding in the loop linkage region (Fig. 1a).

Table 1
The sequence and structure information for the studied molecules.

Molecules	PDB ID	Sequence information	Conformation
24TTG	2GKU	TTGGGTTAGGGTTAGGGTTAGGGA	Hybrid monomer
D-24TTG	self-built	AGGGTTAGGGTTAGGGTTAGGGTTAGGGTTAGGGTTAGGGTTAGGG	Hybrid dimer
dAGRO100	4U5M	TGGTGGTGGTGGTTGTGGTGGTGGTGTT	Intramolecular tandem parallel
GGA8	1OZ8	GGAGGAGGAGGAGGAGGAGGA	
93del	1Y8D	GGGGTGGGAGGAGGGTGGGGTGGGAGGAGGGT	Interlocking parallel
T30695	2LE6	GGGTGGGTGGGTGGGTGGGTGGGTGGGTGGGT	Intermolecular stacked parallel
T30177	2M4P-rebuilt	GTGGTGGGTGGGTGGGTGTGGTGGGTGGGTGGGT	
RHAU	5VHE	SMHPGHLKGREIGMWYAKKQGQKNKEAERQERAVVHMDERREEQIVQLLNSVQAK	/

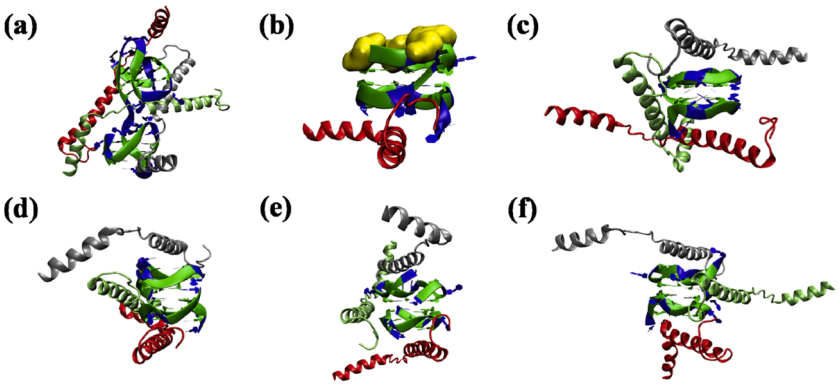

Fig. 1. The representative D-G4s-RHAU structures after docking. (a) D-24TTG-RHAU, (b) dAGRO100-RHAU, (c) GGA8-RHAU, (d) 93del-RHAU, (e) T30695-RHAU, (f) T30177-RHAU. The binding sites were indicated in red for site 1, lime for site 2, and silver for site 3, respectively, with the D-G4s backbone in blue and the dG bases in green.

These binding modes differ from the conventional binding patterns of G4s, which are typically characterized by stacking or groove binding. The specific combination mode indicated the potential for the hybrid dimer to interact with RHAU, which required further illustration by the free energy decomposition in following MD simulation. Furthermore, the unique structural feature of dAGRO100 restricted its interaction to a single binding mode, as demonstrated in Fig. 1b, characterized by stacking at the 3′-end region during docking. Chung et al. [25] have reported that the collapse of thymine residues (highlighted in yellow in Fig. 1b) leads to frustrated binding of RHAU at 5′-end region, further supporting the significant influence of structural specificity on binding site diversity. Conversely, GGA8, 93del, T30695, and T30177 showed similar classical binding modes, including stacking and groove binding, as illustrated in Fig. 1c-f. These multiple binding modes resulted in abundant sites for the interaction between RHAU and D-G4s. Interestingly, the differences brought by structural specificity were clearly reflected in the chromatographic retention behaviors.

3.2. Size exclusion chromatography

Our previous study [44] investigated the differences in retention behavior caused by the binding of RHAU to the D-G4s mentioned above via SEC. Under different D-G4s:RHAU ratios, the D-24TTG-RHAU system exhibited obvious change in retention behavior only at 1:4 (Fig. 2a). There was a noticeable decrease in peak 1 (D-24TTG), followed by an increase in peak 2 belonging to D-24TTG-RHAU complex.

As to dAGRO100 (Fig. 2b), a significant change in chromatograms was observed as soon as the addition of RHAU at 1:1 ratio, with the emergence of a distinct peak (peak 2) for dAGRO100-RHAU complex and a reduction in the intensity of the primary peak (peak 1). Further increasing the RHAU concentration produced no additional changes in retention behavior, indicating that the system was saturated and there was no new complex binding state. Upon incorporating RHAU into GGA8 (Fig. 2c), the peaks of GGA8-RHAU complexes (peaks 2, 3 and 4) with increasingly shorter elution time were observed as the RHAU ratio increased. Notably, at a ratio of 1:4, GGA8 (peak 1) disappeared and transformed completely into the final complex (peak 4). This observation suggested that there was a gradual saturation of structural

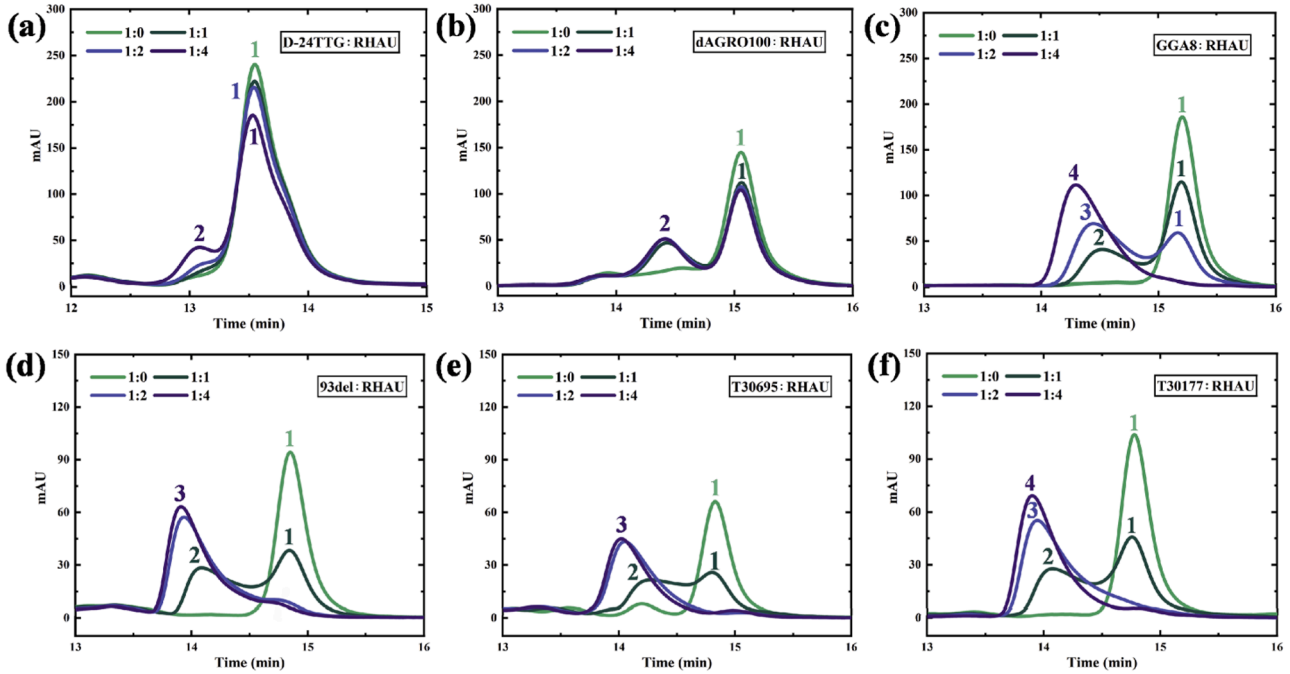

Fig. 2. The overlaid analysis diagram of SEC results under different ratios of D-G4s:RHAU. (a) D-24TTG, (b) dAGRO100, (c) GGA8, (d) 93del, (e) T30695, (f) T30177.

transformation process in this system. Molecular docking revealed the structural divergence between dAGRO100 and GGA8 dictated their distinct RHAU-binding sites richness: single-site versus multi-site. Therefore, there was differential retention behavior for these two D-G4s under varying RHAU concentration conditions.

Although molecular docking observed that 93del, T30695 and T30177 exhibited binding mode similar to that of GGA8, their D-G4s peaks (peak 1) nearly disappeared with the addition of RHAU at 1:2 ratio in SEC, with only stable complex peaks being detected. Both 93del and T30695 demonstrated comparable retention behaviors at ratios of 1:2 and 1:4, indicating that further increasing of RHAU had no obvious effect on the complex state (Fig. 2d-e). In contrast, the complex peak of T30177 (peak 4) remained partially enhanced even at a 1:4 ratio (Fig. 2f).

Given these observed differences in chromatographic retention behavior, a detailed analysis of the binding process was warranted. Thus, the representative structures from molecular docking systems were subjected to subsequent MD simulations, and the results were then employed to further elucidate the binding mechanism underlying the distinct retention behavior.

3.3. Energy calculation and binding mechanism analysis

The MD simulation was performed for 500 ns, and the RMSD analysis indicated the system fluctuated more during the initial 100 ns and reached equilibrium after 150 ns (Figure S3). Thus, the last 200 ns of the trajectory were used for energy analysis (Table 2). It was revealed that 24TTG exhibited negligible binding free energy (−1.51 ± 0.03 kJ/mol), in contrast to the dimer D-24TTG. This result aligns with SEC data, which showed no peak shift upon RHAU addition (Figure S4a), indicating the absence of stable complex formation. Consistently, the binding profiles further confirmed no significant interaction between RHAU and 24TTG (Fig. 3e-g). The trajectory snapshots of 24TTG-RHAU taken at 100 ns intervals further demonstrated that although RHAU folded upon approaching 24TTG, it ultimately failed to bind (Figure S5a-f). All the above indicated that the hybrid monomer was unable to provide the action site for the binding between RHAU and G4s.

However, for D-24TTG, the dimer structure, a special phenomenon was observed: the loop region provided by TTA not only allowed the stacking of the two monomers in a displaced configuration, but more importantly, provided a site for interaction with RHAU (Fig. 3a-b). Meanwhile, the large groove region on the dimer side became another special site for the vertical lateral binding mentioned in docking (Fig. 3c). Hence, D-24TTG exhibited special binding sites compared to its monomer, with binding free energies of −44.21 ± 0.65 kJ/mol (site 1), −28.14 ± 0.41 kJ/mol (site 2), and −53.36 ± 0.44 kJ/mol (site 3). Structural superposition and interaction analysis revealed steric interference among these sites (Fig. 3d). These values were indicative of the relatively weaker binding behavior as observed in the chromatographic analysis. The structural specificity was also reflected in dAGRO100, where RHAU maintained its stacking and binding at the 3′-end throughout the 500 ns simulation (Figure S5l). Compared to D-24TTG, its binding free energy was significantly increased to −94.24 ± 0.95 kJ/mol (Table 2). Although dAGRO100 exhibited a single binding mode, the high binding free energy served as favourable guarantee for the combination, which was fully consistent with its chromatographic retention behavior.

On the contrary, GGA8 was enriched in binding sites (Fig. 3i-k). However, the binding free energies for these various sites were very close to each other, which were −80.88 ± 0.59 kJ/mol (site 1), −80.45 ± 0.55 kJ/mol (site 2), and −76.21 ± 0.64 kJ/mol (site 3), respectively (Table 2). The structures after simulation were analysed by overlapping (Fig. 3l). It was revealed that there was no spatial hindrance interference between binding sites, and the formation of the final stabilized complex was driven by energetic cooperativity. At 1:1 ratio, RHAU bound to one of the three sites and induced conformational stabilization of GGA8. Subsequently, RHAU binding at 1:2 and 1:4 ratios progressively occupied the residual sites, achieving full saturation (Fig. 2c, peak 4). Site binding occurred stochastically, while inter-site cooperativity promoted the formation of the saturated complex.

Since molecular docking showed that 93del, T30177, and T30695 exhibited a similar binding mode as GGA8, we thought that if these three systems also behave like GGA8 to produce the synergistic mechanism with RHAU? To address this question, we conducted further investigations.

As depicted in Figs. 4a-d, 93del, a two-monomer interlocking parallel dimer, exhibited a binding mode to the intramolecular tandem dimer GGA8, involving both stack binding (at the top or bottom) and groove (at the loop) interactions with RHAU. However, the binding free energies differed. Specifically, the bottom stacking binding (−78.04 ± 1.07 kJ/mol) and groove binding (−85.56 ± 1.34 kJ/mol) energies were quite similar, whereas the top stacking binding energy (−107.56 ± 0.57

Table 2
The calculated binding free energies and the individual energy terms for the studied molecules (kJ/mol).

System	Binding sites	Contribution[a]				
		ΔG_{vdw}	ΔG_{ele}	ΔG_{GB}	ΔG_{SA}	ΔG_{Pred}[b]
D-24TTG	1	−27.75 ± 0.55	−172.65 ± 0.63	164.03 ± 0.49	−7.84 ± 0.08	−44.21 ± 0.65
	2	−18.90 ± 0.36	−87.13 ± 0.42	83.27 ± 0.37	−5.38 ± 0.04	−28.14 ± 0.41
	3	−36.90 ± 0.40	−152.56 ± 0.46	144.90 ± 0.39	−8.80 ± 0.05	−53.36 ± 0.44
24TTG	1	−0.21 ± 0.01	−88.89 ± 0.52	87.62 ± 0.50	−0.03 ± 0.01	−1.51 ± 0.03
	2	−0.21 ± 0.01	−88.89 ± 0.52	87.62 ± 0.50	−0.03 ± 0.01	−1.51 ± 0.03
dAGRO100	1	−73.78 ± 0.83	−94.82 ± 0.43	84.67 ± 0.35	−10.31 ± 0.08	−94.24 ± 0.95
GGA8	1	−60.65 ± 0.56	−105.92 ± 0.56	93.89 ± 0.48	−8.20 ± 0.05	−80.88 ± 0.59
	1[c]	−60.57 ± 0.39	−141.15 ± 0.32	116.45 ± 0.25	−8.78 ± 0.04	−94.05 ± 0.41
	2	−59.25 ± 0.54	−99.52 ± 0.55	87.24 ± 0.46	−8.92 ± 0.06	−80.45 ± 0.55
	3	−58.91 ± 0.60	−88.36 ± 0.62	78.53 ± 0.52	−7.47 ± 0.06	−76.21 ± 0.64
93del	1	−60.76 ± 0.87	−89.75 ± 1.07	80.75 ± 0.94	−8.29 ± 0.11	−78.04 ± 1.07
	2	−64.98 ± 1.05	−116.66 ± 1.54	104.53 ± 1.34	−8.45 ± 0.13	−85.56 ± 1.34
	3	−82.26 ± 0.52	−130.07 ± 0.46	115.81 ± 0.38	−11.05 ± 0.06	−107.56 ± 0.57
T30695	1	−88.21 ± 1.52	−111.37 ± 1.80	99.06 ± 1.56	−10.89 ± 0.19	−111.42 ± 1.89
	2	−52.81 ± 1.25	−112.79 ± 2.11	100.63 ± 1.83	−7.07 ± 0.17	−72.05 ± 1.68
	3	−52.83 ± 1.34	−104.13 ± 1.92	93.38 ± 1.65	−6.65 ± 0.16	−70.24 ± 1.73
T30177	1	−103.10 ± 1.83	−135.83 ± 1.87	118.32 ± 1.59	−14.59 ± 0.25	−135.2 ± 2.31
	2	−72.82 ± 1.18	−124.55 ± 1.42	111.17 ± 1.21	−9.10 ± 0.13	−95.30 ± 1.47
	3	−125.47 ± 2.03	−117.07 ± 1.70	103.31 ± 1.47	−16.51 ± 0.26	−155.74 ± 2.46

[a] Mean ± standard errors (SE).
[b] $\Delta G_{Pred} = \Delta G_{vdw} + \Delta G_{ele} + \Delta G_{GB} + \Delta G_{SA}$.
[c] Glu26 mutation to Arg26.

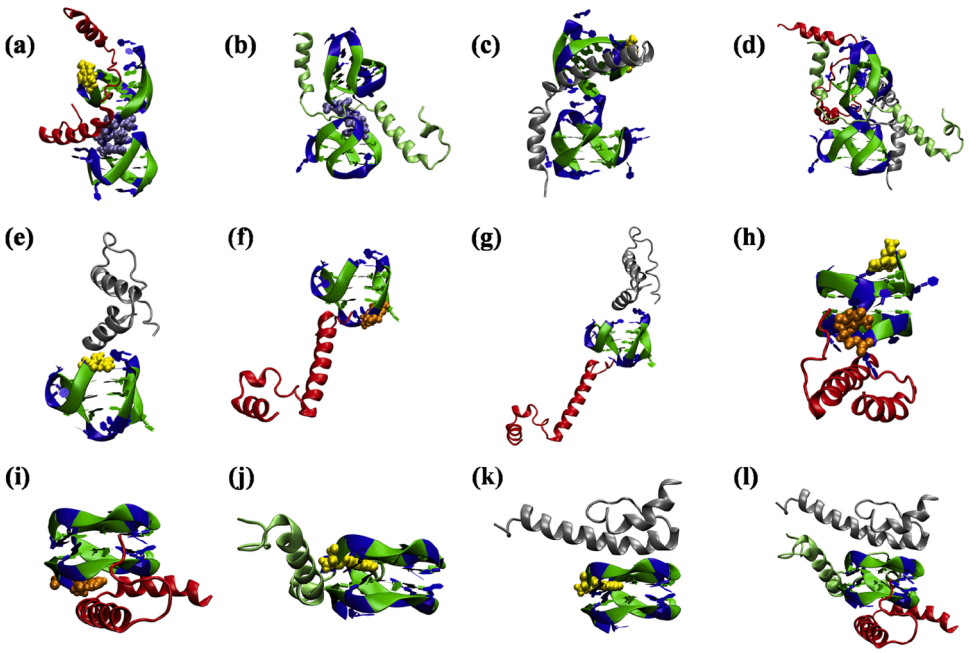

Fig. 3. The final state of structure after 500 ns MD simulation. (a-d) Three binding sites of D-24TTG and their superposition diagram, (e-g) Two potential binding sites of 24TTG and their superimposed diagram, (h) dAGRO100, (i-l) Three binding sites of GGA8 and their superposition diagram. The binding sites were indicated in red for site 1, lime for site 2, and silver for site 3, respectively, with the G4s backbone in blue, the dG bases in green, 3′-end in orange and 5′-end in yellow.

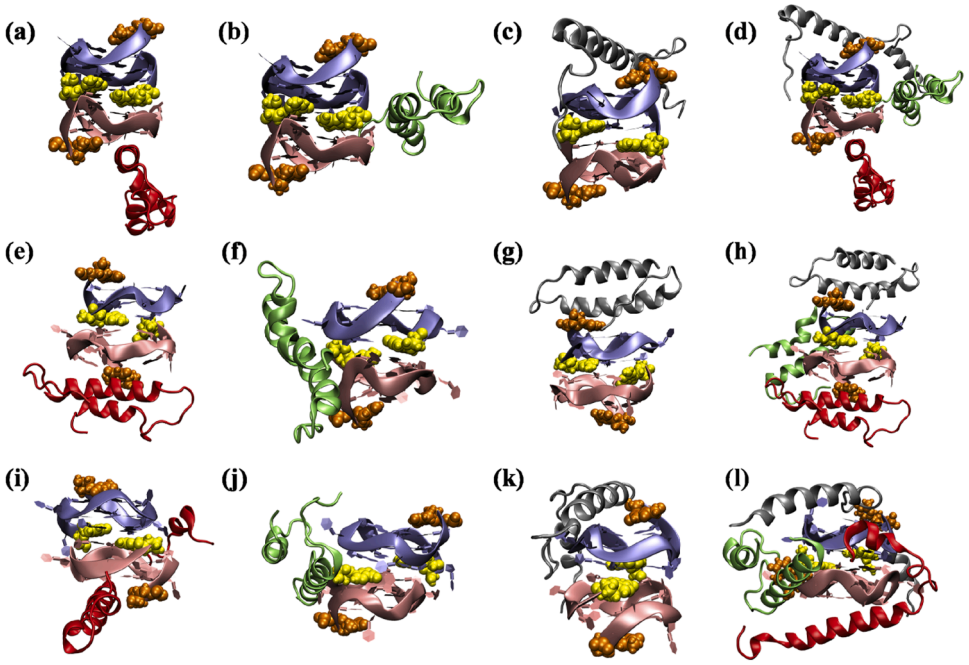

Fig. 4. The final state of structure after 500 ns MD simulation. (a-d) Three binding sites of 93del and their superposition diagram, (e-h) Three binding sites of T30695 and their superimposed diagram, (i-l) Three binding sites of T30177 and their superposition diagram. The binding sites were indicated in red for site 1, lime for site 2, and silver for site 3, respectively, and the monomer A, which composes D-G4s, is pink, monomer B is ice blue, 3′-end in orange and 5′-end in yellow.

kJ/mol) was much higher than the above two binding modes. This notable difference results in a binding mechanism distinct from the GGA8-RHAU system. As a result, at the ratio of 1:1, the top stacking binding was more preferred (Fig. 4c), and the resulting complex corresponded to peak 2 in Fig. 2d. At a 1:2 ratio, both bottom stacking and groove binding were structurally possible. However, a detailed analysis of the 1:1 complex structure revealed that the α-helical region of the pre-bound RHAU molecule (site 3, sliver) occupied spatial coordinates that directly clashed with those required for a second RHAU to engage the lateral groove (Fig. 4d). This made groove binding (site 2, lime) geometrically unfavorable. Therefore, the bottom stacking binding (site 1, red) was more inclined at 1:2 ratio, corresponding to peak 3 in Fig. 2d. When additional RHAU were introduced into the system, the steric hindrance effect prevented any further binding sites from becoming available. This resulted in a more rapid saturation at the 93del-RHAU system, contrasting with the gradual saturation phenomenon observed for GGA8. It was consisted with the phenomenon observed in the SEC experiments. T30695, similar to 93del, could be stably bound by RHAU

via bottom-stacked mode in the 1:1 ratio (Fig. 4e), and its lateral groove binding had the same space-position interactions (shown in Fig. 4f), so the top-stacked binding was more often observed in 1:2 (Fig. 4g).

As to T30177, it was similar with T30695 in conformation, both of them were formed by stacking two monomers on top of each other at the 5′-end. However, T30177 has thymine (dT) bulge near the 5′-end at loop region, which provided more space sites during groove binding. Therefore, T30177 could further combine RHAU at a ratio of 1:4, as observed in SEC results (Fig. 2f). In terms of binding free energy (Table 2), the energy gradient for the three sites of T30177 were −155.74 ± 2.46 kJ/mol (site 3), −135.2 ± 2.31 kJ/mol (site 1) and −95.3 ± 1.47 kJ/mol (site 2), respectively, in descending order. So, as the ratio of RHAU increased, RHAU gradually occupied the available binding sites until saturation, leading to the following binding sequence: top stacking binding at 1:1 ratio (Fig. 4k), bottom stacking binding at 1:2 ratio (Fig. 4i), and the lateral groove binding at 1:4 ratio (Fig. 4j). This finding aligns with the results of Grasso et al., who demonstrated that RG-rich peptides could adopt distinct interaction modes, either primarily through stacking on G-tetrads or binding within the grooves, depending on the structures of the target G4s [45]. The overlapping of the three structures in Fig. 4l confirmed that there is no steric hindrance interference effect among the three binding sites, indicating that the energy difference serves as the driving force for the gradual binding. The distinct energy gradient result in a chromatographic retention behavior for T30177 that differed clearly from those of 93del and T30695.

3.4. Isothermal titration calorimetry verification analysis

To validate the computational results, we performed isothermal titration calorimetry (ITC) experiments to determine the binding affinity (K_d) of D-G4s-RHAU interactions. The ITC-derived K_d values correlated strongly correlation with the MD-derived binding free energies (Fig. 5): systems exhibiting more favorable (more negative) ΔG consistently demonstrated lower (stronger) K_d values.

Specifically, the ITC results of dAGRO100, 93del, and T30695, which yielded sub-micromolar K_d values of 0.28, 0.55, and 0.26 μM, respectively (Fig. 5b, 5d, 5e), confirmed their MD simulations of strong binding interactions (−94.24 ± 0.95 kJ/mol, −107.56 ± 0.57 kJ/mol, −111.42 ± 1.89 kJ/mol). Conversely, among the studied D-G4s, D-24TTG exhibited the weakest experimental affinity (K_d = 4.7 μM, Fig. 5a), consistent with its less favorable calculated ΔG value.

For systems with multiple binding sites, the ITC-derived affinity data closely corresponded to the computationally estimated binding energies. In the case of GGA8, the closely spaced K_d values (1.5 μM, 2.4 μM, 3.8 μM, Fig. 5c) aligned well with the similar ΔG values calculated for its three sites (−80.88 to −76.21 kJ/mol), supporting the observed synergistic, gradual saturation. In contrast, for T30177, the exceptionally broad range of measured K_d values (15 nM, 5.9 μM, 12 μM, Fig. 5f) matched the energy gradient predicted computationally (−95.3 to −155.7 kJ/mol), thereby validating the model of stepwise occupancy driven by this energetic gradient. Furthermore, the two-site binding model and the significant energy difference between the primary and secondary sites for 93del and T30695 predicted by MD were directly corroborated by their respective ITC derived K_{d1} and K_{d2}. The strong agreement between experimental measurements and MD simulations not only confirmed the reliability of computational simulations in predicting relative binding strengths but also revealed their value in elucidating complex multi-site binding mechanisms that underlie the observed SEC phenomena.

3.5. Energy decomposition and contribution

To obtain more information and seek other detailed difference for the binding contribution between RHAU and D-G4s of GGA8, 93del, T30695, and T30177, the energy decomposition analysis was subsequently performed. This analysis focused on peptide residues and D-G4s bases within a 3 Å binding range, utilizing the final 100 ns of the equilibrated trajectory.

For 93del and T30695 (Fig. 6), the electrostatic force served as the dominant binding driver compared to van der Waals force by residues Lys19, Gln22, Lys25, Glu26, Arg29, and Arg32 as the important sites for the RHAU combining to D-G4s. The formation of specific hydrogen bonds substantiates these electrostatic interactions. In the 93del complex, for instance, stable hydrogen bonds formed by Arg29 and Glu26 exhibited occupancies of 45.05 % and 58.05 %, respectively (Table S1), directly contributing to the favorable electrostatic binding component. Conversely, dG and dT, as the main bases for D-G4s binding to RHAU, the contribution to the binding was mainly from van der Waal force. This can be attributed to the existence of layer-to-layer stacking present in the D-G4s system, where the van der Waals effect resulting from the

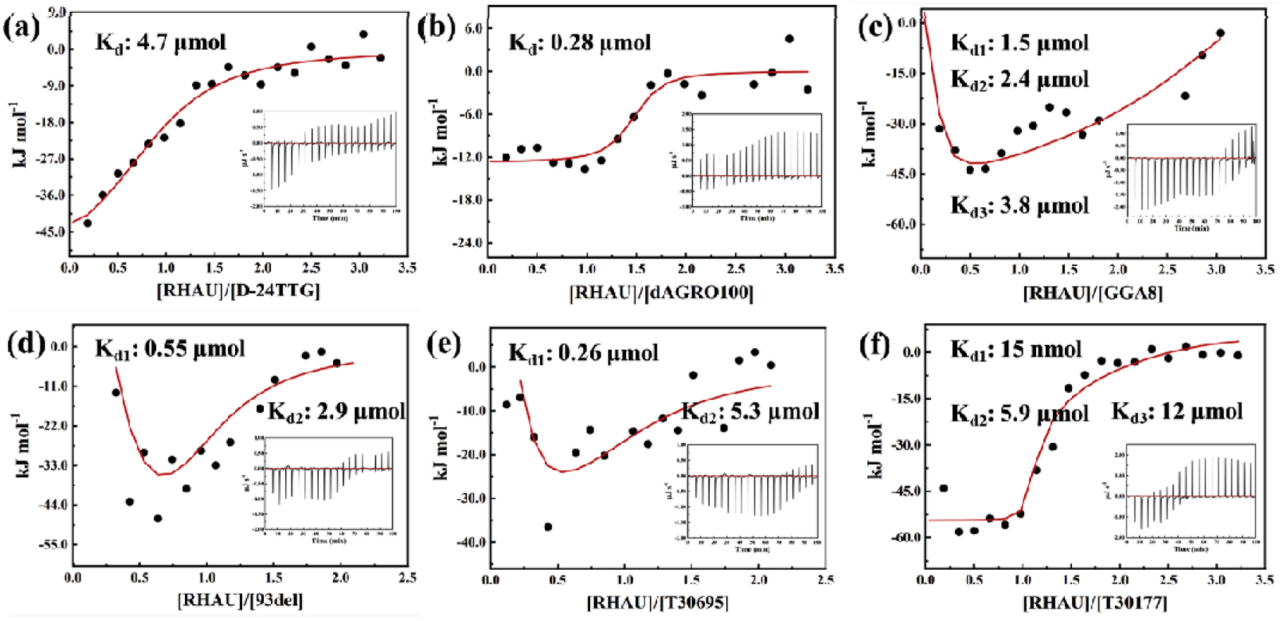

Fig. 5. The isothermal titration calorimetry curves of D-G4s and RHAU. (a) D-24TTG, (b) dAGRO100, (c) GGA8, (d) 93del, (e) T30695, (f) T30177.

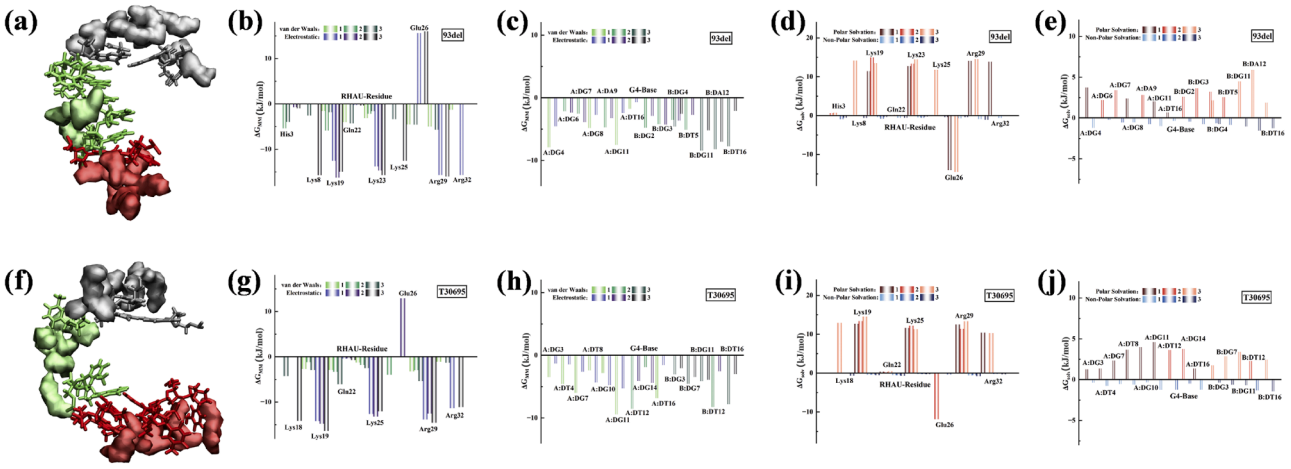

Fig. 6. Energy decomposition analysis between D-G4s key bases and RHAU important residues. (a) Superposition diagram of 93del-RHAU, (b-c) van der Waals and electrostatic interaction diagrams, (d-e) polar and nonpolar interaction diagrams, (f) Superposition diagram of T30695-RHAU, (g-h) van der Waals and electrostatic interaction diagrams, (i-j) polar and nonpolar interaction diagrams.

interplanar stacking structure in D-G4s was more prominent than electrostatic force. Additionally, although polar solvation energies were less favourable for binding, intermolecular forces were sufficient to overcome these solvation effects to promote binding.

Likewise, the electrostatic forces were also the main binding driver for RHAU binding to GGA8 and T30177 compared to van der Waals (shown in Fig. 7). In addition to the key residues mentioned in the 93del and T30695 systems, residues Lys18 and Lys23 were also pivotal in the process of RHAU binding to GGA8 and T30177. Hydrogen bond analysis (Table S1) revealed that Lys18 in GGA8 formed a hydrogen bond with an occupancy of 25.28 %, while Lys23 in T30177 participated in a hydrogen bond with 44.06 % occupancy, corroborating their electrostatic roles. Notably, in the T30177-RHAU system, Arg41 exhibited a strong electrostatic effect, supported by its involvement in a hydrogen bond with 46.04 % occupancy (T30177–1), which contributed to the enhanced binding free energy observed in this complex (Fig. 7*g*). Similarly, the dG base facilitated GGA8 and T30177 binding to the peptide predominantly through van der Waals forces, with the hydrogen bond data also showing generally low or no specific occupancy for bases in van der Waals driven contexts.

In the energy decomposition system described above, residue Glu26 exhibited an extremely strong electrostatic force during D-G4s-RHAU binding, which was detrimental to the stabilisation of complex. Mutating this residue to either Lys or Arg might potentially enhance binding affinity. Considering residue 25 as Lys, MD simulations were performed in the GGA8-site1 system after changing Glu26 to Arg26 (Figure S11). The binding process was remained consistent with that before mutation. However, it was evident from Table 2 that the binding free energy increased to -94.05 ± 0.41 kJ/mol compared to the pre-mutation state (-80.88 ± 0.59 kJ/mol). This mutant system was subjected to energy decomposition and analysed in comparison with the original GGA8-site1 (Fig. 8). Interestingly, residues that were originally not conducive to binding stability became critical for promoting binding, supporting the hypothesis that bio-modification of RHAU peptide can enhance its G4s-binding capability. This finding might offer novel insights into the drug design targeting G4s.

4. Conclusion

MD simulations have revealed that structural diversity of D-G4s led to distinct binding modes with RHAU, as reflected in their chromatographic retention behavior. For instance, the hybrid monomer 24TTG had no binding effect on RHAU, while D-24TTG exhibited weak interaction with RHAU. This difference is attributed to the dislocation stacking of the G-tetrads within the dimer connected by TTA base containing loop regions, resulting in a non-classical vertical binding mode.

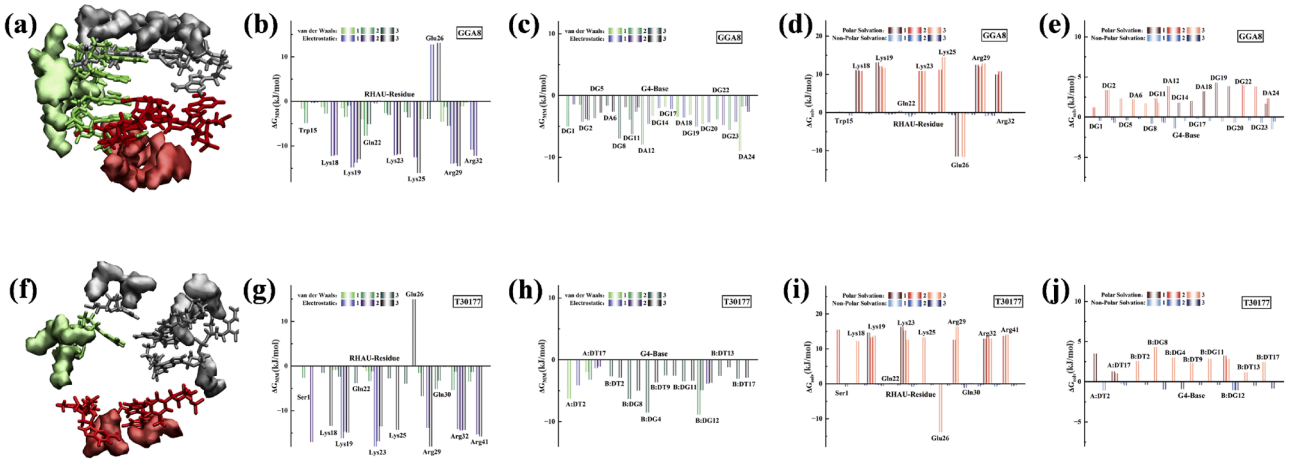

Fig. 7. Energy decomposition contribution between D-G4s key bases and RHAU important residues. (a) Superposition diagram of GGA8-RHAU, (b-c) van der Waals and electrostatic interaction diagrams, (d-e) polar and nonpolar interaction diagrams, (f) Superposition diagram of T30177-RHAU, (g-h) van der Waals and electrostatic interaction diagrams, (i-j) polar and nonpolar interactiondiagrams.

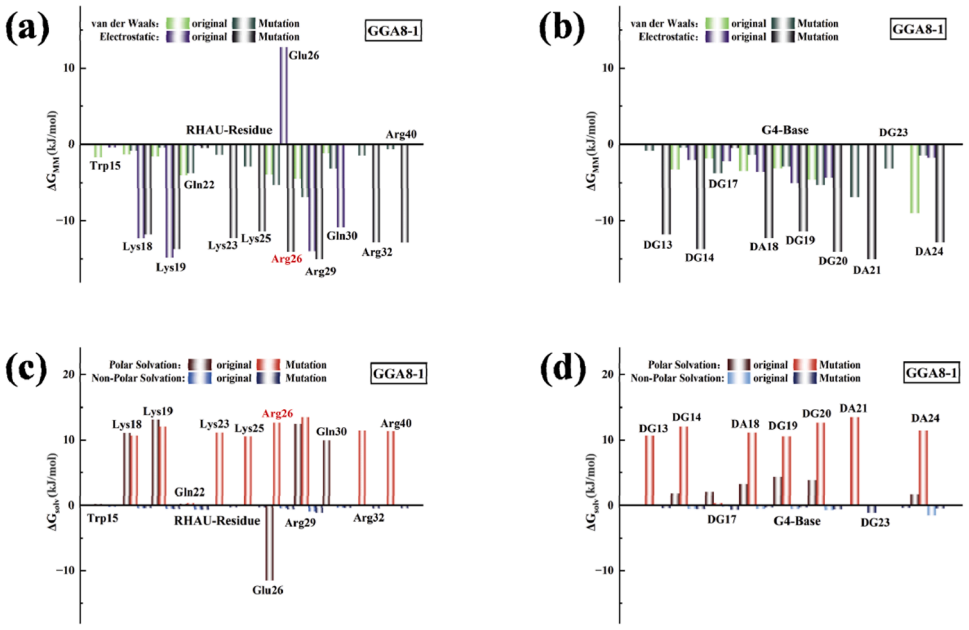

Fig. 8. Energy decomposition contribution of GGA8-site1-RHAU system before and after mutation. (a-b) van der Waals and electrostatic interaction diagrams, (c-d) polar and nonpolar interaction diagrams.

Moreover, the structural specificity brought about by the thymine collapse in dAGRO100 led to a unique binding mode with distinct single binding site compared to GGA8, due to the reduced site enrichment. Besides, while traditional docking predicted similar binding modes for GGA8, 93del, T30695, and T30177, MD simulations combined with ITC results revealed the different binding mechanisms and affinities. For GGA8, the three sites were close in energy, under the synergistic effect, the SEC chromatographic retention showed that the complex system gradually reached saturation as the addition of RHAU increased. In contrast, T30177 also exhibited gradually saturation, but this behavior was governed by the energy gradient difference. T30695 and 93del, instead, were saturated at 1:2 affected by the steric hindrance between the groove binding and the already stabilised binding state sites, which competed with the top stacking. These findings were validated with the affinity data obtained from ITC. Energy decomposition further indicated that the primary driving forces for the binding processes of RHAU and D-G4s: electrostatic forces dominated for RHAU, whereas the main contribution from the D-G4s was van der Waals. Replacing the mutant residue Glu26 with Arg26 markedly increased the binding free energy of the original system. This study elucidates the binding mechanism between D-G4s and RHAU, and clarifies the molecular basis for their distinct SEC retention behavior. These findings not only greatly advance our understanding for RHAU binding to D-G4s, but also provide a new perspective for the investigation on the G4s-binding mechanisms and a conceptual framework for developing therapeutics targeting D-G4s.

CRediT authorship contribution statement

Min Zhu: Writing – original draft, Visualization, Validation, Methodology, Investigation, Formal analysis, Data curation. **Long-yu Zhu:** Methodology, Investigation. **Lu-yan An:** Methodology, Investigation. **Ju Wang:** Methodology, Investigation. **Jun-qin Qiao:** Writing – review & editing, Validation, Resources, Project administration, Funding acquisition, Formal analysis, Conceptualization. **Han-yue Yang:** Resources, Methodology, Investigation. **Wei-juan Zheng:** Formal analysis, Conceptualization. **Hong-zhen Lian:** Writing – review & editing, Supervision, Resources, Funding acquisition, Conceptualization.

Declaration of competing interest

The authors declare that they have no known competing financial interests or personal relationships that could have appeared to influence the work reported in this paper.

Acknowledgement

This work was supported by the National Natural Science Foundation of China (Nos. 22304075, 21577057, 91643105, 21874065 and 22176085), the National Key R&D Program of China (No. 2021YFF0600800). We acknowledge that the numerical calculations in this paper have been done on the computing facilities in the High Performance Computing Center (HPCC) of Nanjing University.

Supplementary materials

Supplementary material associated with this article can be found, in the online version, at doi:10.1016/j.chroma.2026.466706.

Data availability

Data will be made available on request.

References

[1] S. Jonchhe, S. Lahiri, E. Rothenberg, DNA G-quadruplexes: structural and functional insights, DNA Repair (Amst.) 156 (2025) 103910.
[2] L. Chen, J. Dickerhoff, K.W. Zheng, S. Erramilli, H. Feng, G. Wu, B. Onel, Y. Chen, K.B. Wang, M. Carver, C. Lin, S. Sakai, J. Wan, C. Vinson, L. Hurley, A. A. Kossiakoff, N. Deng, Y. Bai, N. Noinaj, D. Yang, Structural basis for nucleolin recognition of *MYC* promoter G-quadruplex, Science 388 (6744) (2025) eadr1752.
[3] B. Onel, C. Lin, D. Yang, DNA G-quadruplex and its potential as anticancer drug target, Sci. China Chem. 57 (12) (2014) 1605–1614.
[4] G.F. Soudeh, A. Atefe, B. Aria, M.H. Bashdar, T. Mohammad, J. Elena, E.D. Marcel, Interaction between non-coding RNAs, mRNAs and G-quadruplexes, Cancer Cell Int. 22 (1) (2022) 171.
[5] F.Y. Teng, Z.Z. Jiang, M. Guo, X.Z. Tan, F. Chen, X.G. Xi, Y. Xu, G-quadruplex DNA: a novel target for drug design, Cell. Mol. Life Sci. 78 (19) (2021) 6557–6583.
[6] I. Frasson, V. Pirota, S.N. Richter, F. Doria, Multimeric G-quadruplexes: a review on their biological roles and targeting, Int. J. Biol. Macromol. 204 (2022) 89–102.
[7] T.C. Liao, T.Z. Ma, Z. Liang, X.T. Zhang, C.Y. Luo, L. Liu, C.Q. Zhou, A comparative study on high selectivities of human telomeric dimeric G-quadruplexes by dimeric G-quadruplex binders, Chemistry (Easton) 24 (59) (2018) 15840–15851.

[8] C. Liu, Q. Wang, L. Shi, T. Li, Robust G-quadruplex dimer-guided transmembrane DNA nanovehicles for targeted payload delivery, Anal. Sens. 5 (1) (2025) e202400048.
[9] E.P. Booy, M. Meier, N. Okun, S.K. Novakowski, S. Xiong, J. Stetefeld, S. A. McKenna, The RNA helicase RHAU (DHX36) unwinds a G4-quadruplex in human telomerase RNA and promotes the formation of the P1 helix template boundary, Nucleic Acids Res. 40 (9) (2012) 4110–4124.
[10] X. Huang, K. Zhao, M. Jiang, D. Qiu, J. Zhou, Z. Yang, The G4 resolvase RHAU regulates ventricular trabeculation and compaction through transcriptional and post-transcriptional mechanisms, J. Biol. Chem. 298 (1) (2022) 101449.
[11] M. Trajkovski, M.W. Silva, J. Plavec, Unique structural features of interconverting monomeric and dimeric G-quadruplexes adopted by a sequence from the intron of the N-myc Gene, J. Am. Chem. Soc. 134 (9) (2012) 4132–4141.
[12] S. Koit, N. Tamberg, A. Reinapae, L. Peil, A. Kristjuhan, I. Ilves, A conserved phosphorylation mechanism for regulating the interaction between the CMG replicative helicase and its forked DNA substrate, J. Biol. Chem. 301 (4) (2025) 108408.
[13] T. Urata, F. Kimura, K. Ohshima, K. Ikehata, M. Yamaguchi, K. Ishii, Immunohistochemistry and machine learning study of DNA replication-associated proteins in uterine epithelial tumors and precursor lesions, Acta Histochem. 127 (2) (2025) 152251.
[14] J. Figueiredo, J.L. Mergny, C. Cruz, G-quadruplex ligands in cancer therapy: progress, challenges, and clinical perspectives, Life Sci. 340 (2024) 122481.
[15] K.B. Wang, Y. Wang, J. Dickerhoff, D. Yang, DNA G-quadruplexes as targets for natural product drug discovery, Engineering 38 (2024) 39–51.
[16] C. Honisch, E. Ragazzi, R. Hussain, J. Brazier, G. Siligardi, P. Ruzza, Interaction of a short peptide with G-quadruplex-forming sequences: an SRCD and CD study, Pharmaceutics 13 (8) (2021) 1104.
[17] R.D. Villar-Guerra, J.O. Trent, J.B. Chaires, G-quadruplex secondary structure obtained from circular dichroism spectroscopy, Angew. Chem. Int. Ed. 57 (24) (2018) 7171–7175.
[18] B. Heddi, V.V. Cheong, E. Schmitt, Y. Mechulam, A.T. Phan, Recognition of different base tetrads by RHAU (DHX36): x-ray crystal structure of the G4 recognition motif bound to the 3′-end tetrad of a DNA G-quadruplex, J. Struct. Biol. 209 (1) (2020) 107399.
[19] M. Meier, A.M. Torres, N.J. Krahn, M.D. McDougall, G.L. Orriss, E.K. McRae, E. P. Booy, K. McEleney, T.R. Patel, S.A. McKenna, J. Stetefeld, Structure and hydrodynamics of a DNA G-quadruplex with a cytosine bulge, Nucleic Acids Res. 46 (10) (2018) 5319–5331.
[20] D.T. Dang, A.T. Phan, Development of fluorescent protein probes specific for parallel DNA and RNA G-quadruplexes, ChemBioChem. 17 (1) (2016) 42–45.
[21] J. Wang, J.Q. Qiao, W.J. Zheng, H.Z. Lian, Study on the interaction of a peptide targeting specific G-quadruplex structures based on chromatographic retention behavior, Int. J. Mol. Sci. 24 (2) (2023) 1438.
[22] S. Chaudhary, M. Kumar, M. Kaushik, Interface of G-quadruplex with both stabilizing and destabilizing ligands for targeting various diseases, Int. J. Biol. Macromol. 219 (2022) 414–427.
[23] S.A. Hollingsworth, R.O. Dror, Molecular dynamics simulation for all, Neuron 99 (6) (2018) 1129–1143.
[24] K.i. Shinohara, Y. Sannohe, S. Kaieda, K.i. Tanaka, H. Osuga, H. Tahara, Y. Xu, T. Kawase, T. Bando, H. Sugiyama, A chiral wedge molecule inhibits telomerase activity, J. Am. Chem. Soc. 132 (11) (2010) 3778–3782.
[25] W.J. Chung, B. Heddi, E. Schmitt, K.W. Lim, Y. Mechulam, A.T. Phan, Structure of a left-handed DNA G-quadruplex, Proc. Natl. Acad. Sci. U. S. A. 112 (9) (2015) 2729–2733.
[26] A. Matsugami, T. Okuizumi, S. Uesugi, M. Katahira, Intramolecular higher order packing of parallel quadruplexes comprising a G:G:G:G tetrad and a G(:A):G(:A):G(:A):G heptad of GGA triplet repeat DNA, J. Biol. Chem. 278 (30) (2003) 28147–28153.
[27] A.T. Phan, V. Kuryavyi, J.B. Ma, A. Faure, M.L. Andréola, D.J. Patel, An interlocked dimeric parallel-stranded DNA quadruplex: a potent inhibitor of HIV-1 integrase, Proc. Natl. Acad. Sci. U. S. A. 102 (3) (2005) 634–639.
[28] N.Q. Do, K.W. Lim, M.H. Teo, B. Heddi, A.T. Phan, Stacking of G-quadruplexes: NMR structure of a G-rich oligonucleotide with potential anti-HIV and anticancer activity, Nucleic Acids Res. 39 (21) (2011) 9448–9457.
[29] V.T. Mukundan, N.Q. Do, A.T. Phan, HIV-1 integrase inhibitor T30177 forms a stacked dimeric G-quadruplex structure containing bulges, Nucleic Acids Res. 39 (20) (2011) 8984–8991.
[30] K.N. Luu, A.T. Phan, V. Kuryavyi, L. Lacroix, D.J. Patel, Structure of the human telomere in K^+ solution: an intramolecular (3 + 1) G-quadruplex scaffold, J. Am. Chem. Soc. 128 (30) (2006) 9963–9970.
[31] S. Yuan, H.C. Chan, Z. Hu, Using PyMOL as a platform for computational drug design, WIREs Comput. Mol. Sci. 7 (2) (2017) e1298.
[32] L.P. Patro, A. Kumar, N. Kolimi, T. Rathinavelan, 3D-NuS: a web server for automated modeling and visualization of non-canonical 3-dimensional nucleic acid structures, J. Mol. Biol. 429 (16) (2017) 2438–2448.
[33] H.M. Berman, J. Westbrook, Z. Feng, G. Gilliland, T.N. Bhat, H. Weissig, I. N. Shindyalov, P.E. Bourne, The protein data bank, Nucleic Acids Res. 28 (1) (2000) 235–242.
[34] Y. Yan, D. Zhang, P. Zhou, B. Li, S.Y. Huang, HDOCK: a web server for protein-protein and protein-DNA/RNA docking based on a hybrid strategy, Nucleic Acids Res. 45 (W1) (2017) W365–W373.
[35] P. Mark, L. Nilsson, Structure and dynamics of the TIP3P, SPC, and SPC/E water models at 298 K, J. Phys. Chem. A 105 (43) (2001) 9954–9960.
[36] J.A. Maier, C. Martinez, K. Kasavajhala, L. Wickstrom, K.E. Hauser, C. Simmerling, ff14SB: improving the accuracy of protein side chain and backbone parameters from ff99SB, J. Chem. Theory Comput. 11 (8) (2015) 3696–3713.
[37] M.J. Abraham, T. Murtola, R. Schulz, S. Páll, J.C. Smith, B. Hess, E. Lindahl, GROMACS: high performance molecular simulations through multi-level parallelism from laptops to supercomputers, SoftwareX 1-2 (2015) 19–25.
[38] S. Páll, A. Zhmurov, P. Bauer, M. Abraham, M. Lundborg, A. Gray, B. Hess, E. Lindahl, Heterogeneous parallelization and acceleration of molecular dynamics simulations in GROMACS, J. Chem. Phys. 153 (13) (2020) 134110.
[39] T. Darden, D. York, L. Pedersen, Particle mesh Ewald: an N·log(N) method for Ewald sums in large systems, J. Chem. Phys. 98 (12) (1993) 10089–10092.
[40] D.J. Keffer, C. Baig, P. Adhangale, B.J. Edwards, A generalized Hamiltonian-based algorithm for rigorous equilibrium molecular dynamics simulation in the canonical ensemble, J. Non-Newtonian Fluid Mech. 152 (1) (2008) 129–139.
[41] W. Humphrey, A. Dalke, K. Schulten, VMD: visual molecular dynamics, J. Mol. Graph. 14 (1) (1996) 33–38.
[42] B.R. Miller, T.D. McGee, J.M. Swails, N. Homeyer, H. Gohlke, A.E. Roitberg, MMPBSA.Py: an efficient program for end-state free energy calculations, J. Chem. Theory Comput. 8 (9) (2012) 3314–3321.
[43] M.S. Valdés-Tresanco, M.E. Valdés-Tresanco, P.A. Valiente, E. Moreno, gmx_MMPBSA: a new tool to perform end-state free energy calculations with GROMACS, J. Chem. Theory Comput. 17 (10) (2021) 6281–6291.
[44] J. Wang, J.Q. Qiao, C. Liang, X.W. Guo, M.Y. zhang, W.J. Zheng, H.Z. Lian, Exploring the interactions between RHAU peptide and G-quadruplex dimers based on chromatographic retention behaviors, Molecules 29 (24) (2024) 5915.
[45] N. Grasso, R. Graziano, S. Marzano, F. D'Aria, F. Merlino, P. Grieco, A. Randazzo, B. Pagano, J. Amato, Unveiling the interaction between DNA G-quadruplexes and RG-rich peptides, Int. J. Biol. Macromol. 253 (2023) 126749.